ISROMAC 2017
International Symposium on Transport Phenomena
and Dynamics of Rotating Machinery
Maui, Hawaii
December 16-21, 2017

[Extended Abstract]

Effect of Fan on Inlet distortion: A Mixed fidelity Approach

Yunfei Ma, Jiahuan Cui, Nagabhushana Rao Vadlamani, Paul Tucker
Department of Engineering, University of Cambridge, United Kingdom

1. Introduction

Flow distortion is typically encountered on the engine intakes and in the duct flows. With such distorted flow, the fan performance could be significantly deteriorated. Interestingly, the presence of a fan is also shown to affect the distortion recovery ([1]). To numerically investigate this interaction, it is crucial to resolve the following flow regimes: (a) the separated flow region and (b) the influence of a fan.

Most research in literature addressed the fan-distortion study using low fidelity methods such as URANS and RANS [2, 3, 4]. It is well known that the predictive capability of these low fidelity approaches are satisfactory at the design point. However, they still suffer from severe limitations under off-design conditions including flow separation, distortion and unsteadiness [5, 6, 7]. For flows under these conditions, eddy resolving simulations such as DNS/LES and hybrid LES/RANS are demonstrated to yield more promising results [7, 8].

On the other hand, the fan influence can be represented either by resolving all fan blades or with a body force. While the former approach is computationally expensive [9], the Body Force Method (BFM) is shown to be much more economical[10].

In order to accurately investigate the fan influence on the inlet distortion at reasonable computational expense, the current study employs a mixed fidelity approach. The unsteady separated regime is captured using a high-fidelity eddy resolving approach while the fan effect is modelled using the body force. Subsequently, the recovery of distortion in the presence of a fan is examined using both the mean and turbulent characteristics.

2. Numerical Framework

Figure 1 illustrates the computational domain and the boundary conditions considered in the current study. It features a distortion generator ('beam') of height 'H' placed at an axial distance of '$12.5H$' from the inlet. The fan is positioned at a streamwise distance of 5.25H from the beam. This simplified set up is motivated by the experimental studies on the Darmstadt Rotor [11], albeit under different operating conditions. All the spatial quantities mentioned in the following sections are normalised by the beam height H. The velocity is normalised by the velocity u_∞ measured at the maximum height of the beam (Fig.1), which corresponds to the outer edge velocity of a separating shear layer.

The beam is represented using the conventional IBM [12]. The separated flow downstream of the beam is captured using the eddy resolving approach, while the force field of a rotating fan is replicated using a smeared IBM (IBMSG, i.e. IBM for Smeared Geometries [13]). This approach avoids the need to capture detailed blade geometry or incorporate moving boundaries. Instead, it represents

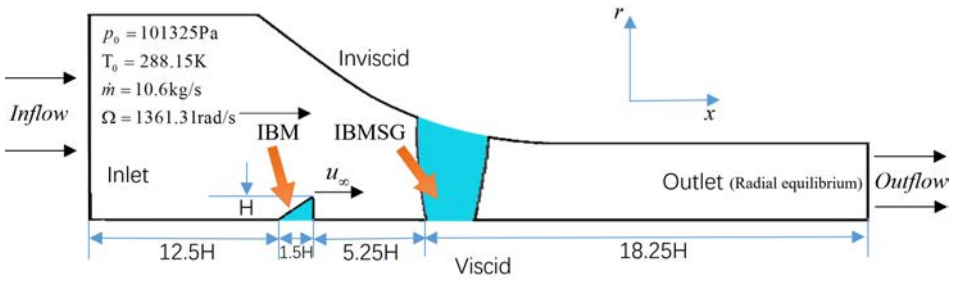

Figure 1. Experiment settings

the force field generated by the rotating fan blades and captures the suction effect of the fan, thereby substantially reducing computational cost.

The present simulations are carried out using a Rolls-Royce's in-house CFD code, HYDRA. Both IBM and IBMSG are implemented into the numerical framework and are thoroughly validated [1].

3. Results

3.1 Instantaneous flow field

Figure 2 shows the contours of the stagnation pressure. It demonstrates both the distortion generated in the lee of the beam and an increase in the stagnation pressure due the presence of the fan. Figure 3

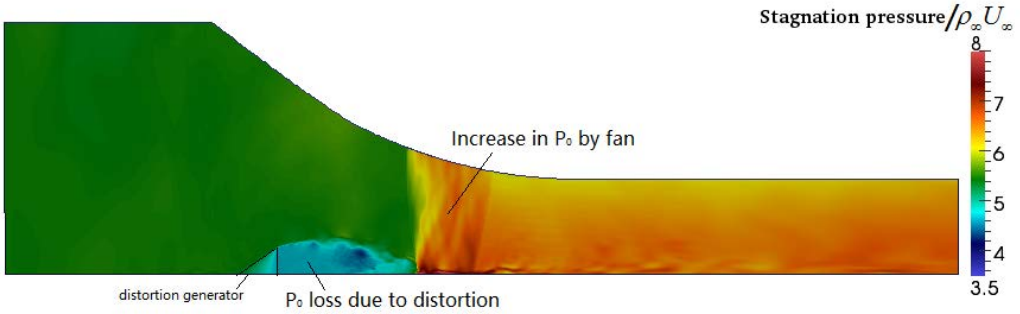

Figure 2. Total pressure distribution

and 4 demonstrates the effect of fan on the instantaneous flow using the iso-surfaces of Q, contoured with the local axial velocity. The axial location of the fan is also shown by means of a sketch. Coherent two-dimensional detached shear layer forms at the edge of the beam which rapidly destabilized downstream. A decrease in the recirculation region is clearly evident in the presence of the fan. Qualitatively, an increase in the length scales of the turbulent structures due to fan is notable from Fig. 4.

4. Time averaged flow field

Figure 5 compares the mean velocity profiles at different streamwise locations on a carpet plot. A line joining the locus of inflectional points of the velocity profiles is also overlaid. As noted from the instantaneous flow, the extent of the recirculation zone is significantly reduced due to the fan. The flow reattaches at an axial location which is more than a beam height upstream of the fan leading edge.

Figure 6a shows the contours of the time-averaged turbulent kinetic energy (TKE, left: no fan; right: with fan). The TKE in the shear layer and in the reattaching regime has increased by around 40-70% in the axial direction in the presence of fan. This is partially caused by a higher production

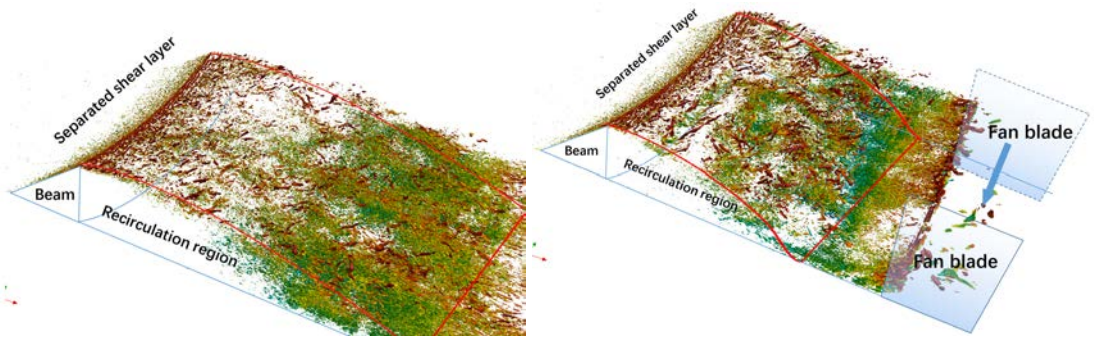

Figure 3. Instantenous flow for the case without fan and with fan

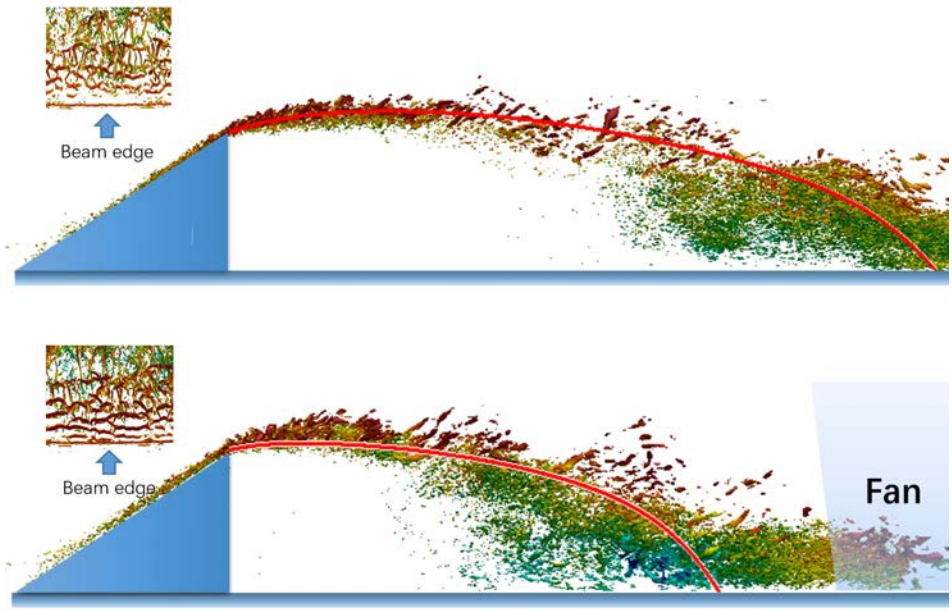

Figure 4. Lateral view of instantenous flow for the case without fan and with fan

in the shear layer (Fig. 6b) and partially by a stronger convection in the middle-rear part of the recirculation region (Fig. 6c).

4.1 Mechanism

This section delves into the mechanism by which the fan has reduced the recirculation region. Figure 6b and 6c compare the contours of TKE production and convection without/with fan. A substantial increase in both terms is notable from the figure. To examine this in more details, the individual contributions from the dominant terms (in order): $\langle u'u' \rangle \, \partial U/\partial x$, $\langle v'v' \rangle \, \partial V/\partial y$ and $\langle u'v' \rangle \, \partial U/\partial y$ to the TKE production are analysed. Both the velocity gradients and the corresponding Reynolds stresses from these contributions are shown in figures 8a,9a and 10a respectively. The direct effect of the fan is observable between $x = 2H - 4H$ in Figure 9a, where the wall-normal Reynolds stresses are much larger. We consider this to be a 'direct effect'. On the other hand, there is an increase in both the streamwise and wall normal fluctuations within the shear layer at the edge of the beam between $x = 0 - 2H$ in Figure 8a and 10a. This is attributed to the 'indirect effect' of the fan, where the turbulence generated in the vicinity of the fan is fed back to the shear layer. Such feedback effect can be seen in both the convection (Fig. 6c) and the z-vorticity (Fig. 7). The contribution from the TKE production is dominated by the Reynolds stresses, while that by the velocity gradients is secondary. More details will be provided in the final manuscript.

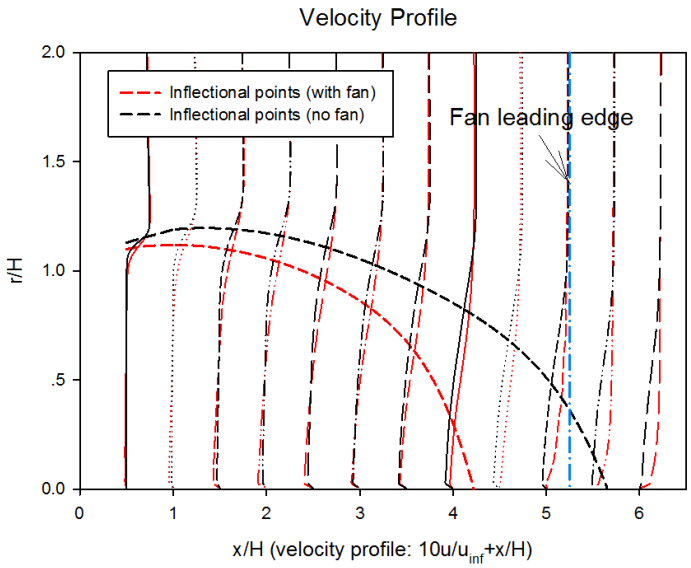

Figure 5. Velocity profile

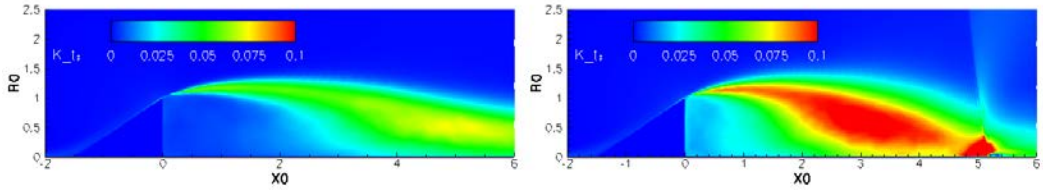

(a) Contours of TKE

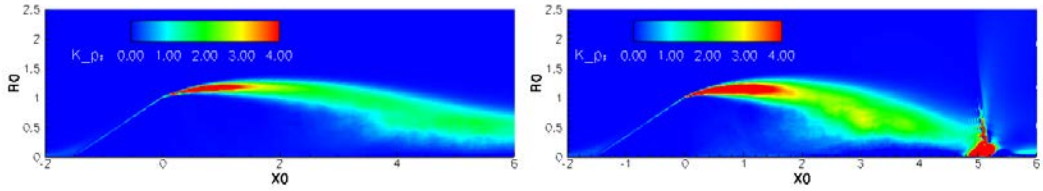

(b) Contours of TKE Production

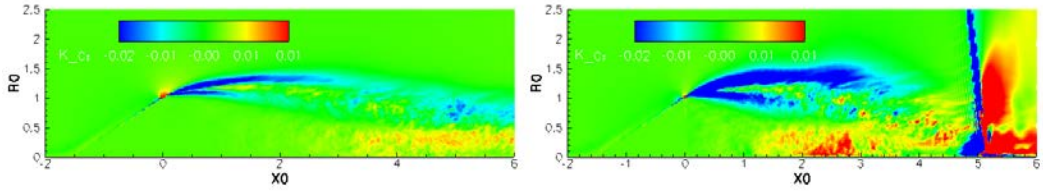

(c) Contours of TKE convection

Figure 6. Turbulent Kinetic Energy Statistics

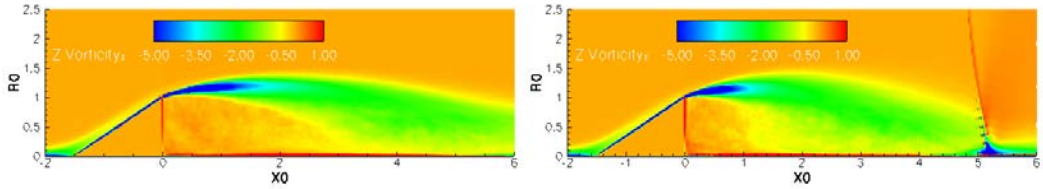

Figure 7. Z-vorticity

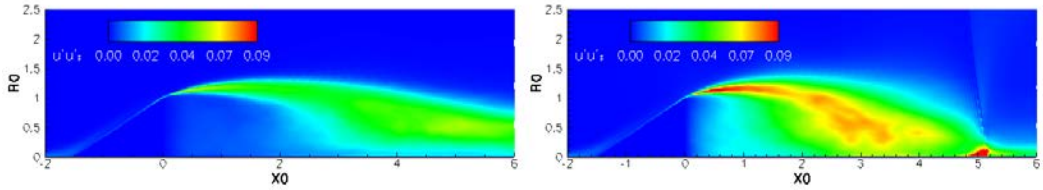

(a) Reynolds stress $\langle u'u' \rangle$

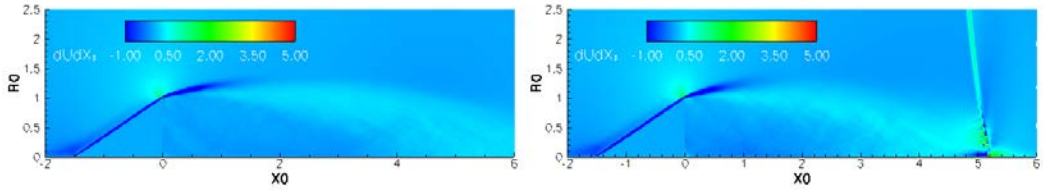

(b) Velocity gradient $\partial U/\partial x$

Figure 8. TKE production term $\langle u'u' \rangle \, \partial U/\partial x$

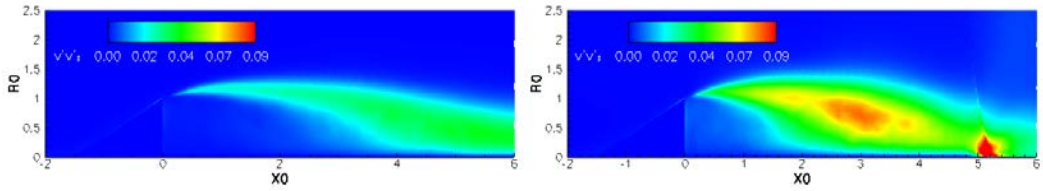

(a) Reynolds stress $\langle v'v' \rangle$

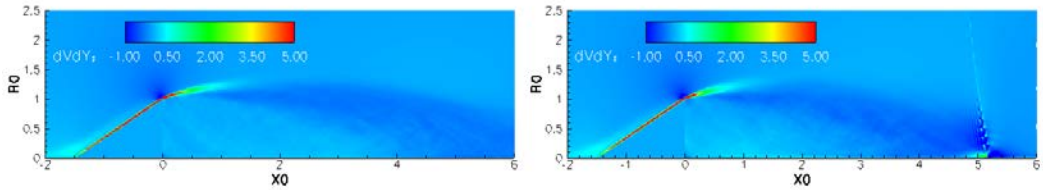

(b) Velocity gradient $\partial V/\partial y$

Figure 9. TKE production term $\langle v'v' \rangle \, \partial V/\partial y$

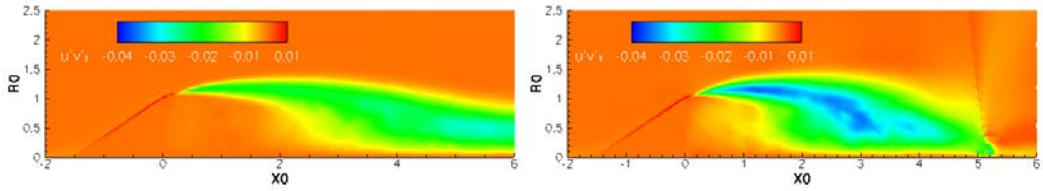

(a) Reynolds stress $\langle u'v' \rangle$

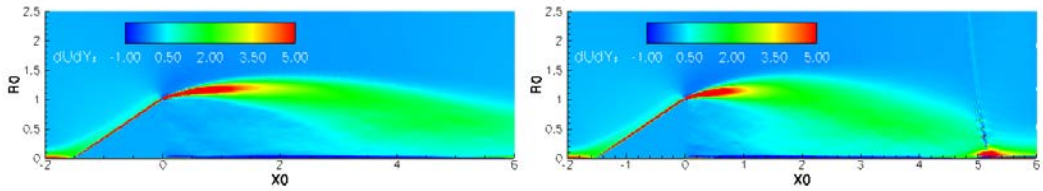

(b) Velocity gradient $\partial U/\partial y$

Figure 10. TKE production term $\langle u'v' \rangle \, \partial U/\partial y$

References

[1] Teng Cao, Nagabhushana Rao Vadlamani, Paul G Tucker, Angus R Smith, Michal Slaby, and Christopher TJ Sheaf. Fan–intake interaction under high incidence. *Journal of Engineering for Gas Turbines and Power*, 139(4):041204, 2017.

[2] V Jerez Fidalgo, CA Hall, and Y Colin. A study of fan-distortion interaction within the nasa rotor 67 transonic stage. *Journal of Turbomachinery*, 134(5):051011, 2012.

[3] Sebastian Barthmes, Jakob P Haug, Andreas Lesser, and Reinhard Niehuis. Unsteady cfd simulation of transonic axial compressor stages with distorted inflow. In *Advances in Simulation of Wing and Nacelle Stall*, pages 303–321. Springer, 2016.

[4] John Seddon and Eustace Laurence Goldsmith. *Intake aerodynamics*. Amer Inst of Aeronautics &, 1999.

[5] Paul Tucker and Yan Liu. Turbulence modeling for flows around convex features. In *44th AIAA Aerospace Sciences Meeting and Exhibit*, page 716, 2006.

[6] Nicolas Gourdain, Laurent YM Gicquel, and Elena Collado. Comparison of rans and les for prediction of wall heat transfer in a highly loaded turbine guide vane. *Journal of propulsion and power*, 28(2):423–433, 2012.

[7] Yangwei Liu, Hao Yan, Lipeng Lu, and Qiushi Li. Investigation of vortical structures and turbulence characteristics in corner separation in a linear compressor cascade using ddes. *Journal of Fluids Engineering*, 139(2):021107, 2017.

[8] PR Spalart and DR Bogue. The role of cfd in aerodynamics, off-design. *The Aeronautical Journal (1968)*, 107(1072):323–329, 2003.

[9] Jeffrey Slotnick, Abdollah Khodadoust, Juan Alonso, David Darmofal, William Gropp, Elizabeth Lurie, and Dimitri Mavriplis. Cfd vision 2030 study: a path to revolutionary computational aerosciences. 2014.

[10] Roberto Verzicco, Jamaludin Mohd-Yusof, Paolo Orlandi, and Daniel Haworth. Large eddy simulation in complex geometric configurations using boundary body forces. *AIAA journal*, 38(3):427–433, 2000.

[11] Fabian Wartzek, Felix Holzinger, Christoph Brandstetter, and Heinz-Peter Schiffer. Realistic inlet distortion patterns interacting with a transonic compressor stage. In *Advances in Simulation of Wing and Nacelle Stall*, pages 285–302. Springer, 2016.

[12] Charles S Peskin. The immersed boundary method. *Acta numerica*, 11:479–517, 2002.

[13] Teng Cao, Paul Hield, and Paul G Tucker. Hierarchical immersed boundary method with smeared geometry. In *54th AIAA Aerospace Sciences Meeting*, page 2130, 2016.